

# Efficient, Adaptive Near-Field Beam Training based on Linear Bandit

Junchi Liu, Zijun Wang, Rui Zhang, *member, IEEE*

**Abstract**—This letter proposes a linear bandit-based beam training framework for near-field communication under multipath channels. By leveraging Thompson Sampling (TS), the framework adaptively balances exploration and exploitation to maximize cumulative beamforming gain under limited pilot overhead. To ensure data-efficient learning, we incorporate a correlated Gaussian prior in the DFT domain, using a Gaussian kernel to capture spatial correlations and near-field energy leakage. We develop three TS strategies: codebook-constrained search for rapid convergence via structural regularization, continuous-space search to achieve near-optimal performance, and a two-stage hybrid refinement scheme that balances convergence speed and estimation accuracy. Simulation results show that the proposed framework reduces pilot overhead by up to 90% while achieving more than a 2dB SNR gain over baselines in multipath environments. Furthermore, the continuous-space search is shown to be asymptotically optimal, approaching the full-CSI bound when the pilot overhead is unconstrained.

**Index Terms**—near-field, beam training, Linear Bandit, Thompson Sampling

## I. INTRODUCTION

THE emerging 6G ecosystem will utilize high-frequency bands such as upper mid band, millimeter-wave (mmWave) and terahertz (THz) bands to meet surging capacity demands [1], [2], [3], [4]. A key enabler for this is extremely large-scale MIMO (XL-MIMO), which employs very large antenna apertures to overcome severe propagation loss. However, large apertures significantly extend the radiative near-field region, where the traditional far-field planar-wave assumption becomes invalid [5]. In this region, channel steering vectors are characterized by spherical wavefronts and must be parameterized by both angle and distance for precise beam focusing [6], [7].

Near-field beam training typically necessitates exhaustive sweeping over a two-dimensional polar-domain codebook [8]. However, the additional distance dimension leads to a codebook size that scales drastically, incurring prohibitive pilot overhead and training latency [9], [10]. To mitigate this, several efficient strategies have been proposed, often assuming a dominant Line-of-Sight (LoS) path. One representative line of work adopts hierarchical search [11], [12] to progressively refine the beam direction and distance without scanning the full 2D codebook. For instance, [12] proposed a two-stage hierarchical beam training procedure that first searches in the angular domain and then refines the estimate in the polar (angle–range) domain, thereby avoiding

exhaustive 2D sweeps. Another line relies solely on far-field DFT beams and infers the range through the intrinsic angle–range coupling. For example, [13], [14] enable joint angle-and-range estimation via beamwidth information, effectively bypassing 2D polar-domain scanning. Beyond deterministic search, sequential learning methods based on Bayesian optimization have also been explored to reduce sweeping overhead further. For instance, the Upper Confidence Bound (UCB) framework in [15] models the beam response over near-field codewords using Gaussian process regression; by exploiting the smooth spatial correlation of the channel, such bandit-based methods balance exploration and exploitation to achieve accurate alignment with a small number of pilots [16]. While effective in reducing overhead, these methods often overlook the impact of multipath propagation. In practice, particularly in indoor, cluttered, or lower-frequency environments such as the upper mid-band, XL-MIMO channels are rarely pure LoS. To address the multipath challenge, a multi-beam linear-combination method is proposed in [17]. By adaptively combining multiple beams based on user-side feedback of the received signal’s amplitude and phase, this approach effectively captures significant propagation paths. However, this approach fundamentally relies on an exhaustive sweep of the entire codebook to ensure reconstruction accuracy, resulting in a pilot overhead comparable to that of traditional methods and limiting its utility in latency-sensitive applications.

Consequently, how to achieve robust beam alignment under multipath conditions with low pilot overhead is a critical problem. To fill this gap, we propose a linear bandit beam training framework that employs Thompson Sampling (TS) to maximize cumulative beamforming gain under strict pilot constraints. This method can adaptively balance exploration and exploitation. Considering near-field energy leakage effects in angular domain, we construct the prior covariance matrix using a Gaussian kernel, which can model angular channel correlations and accelerate posterior convergence. Furthermore, we develop three TS-based strategies: a codebook-constrained search for rapid initial stabilization, a continuous-space search for high-precision alignment, and a hybrid refinement scheme that adaptively balances training speed and accuracy.

The rest of the paper is organized as follows. Section II introduces the system model in the spatial domain and DFT domain. Section III proposes three TS-based beam training schemes. Section IV analyzes the simulation results and benchmarks our algorithm with the multi-beam combination approach in [17] and exhaustive near-field codebook search. Section V draws the conclusion of the work.

## II. SYSTEM MODEL

We consider a system where a base station (BS) equipped with an  $N$ -element uniform linear array (ULA) serves a

Junchi Liu, Zijun Wang and Rui Zhang are with the Department of Electrical Engineering, The State University of New York at Buffalo, New York, USA (email: junchili@buffalo.edu, zwang267@buffalo.edu, rzhang45@buffalo.edu).

This work was supported in part by the CSD, MediaTek Inc. USA, under Grant 103764, and in part by the National Science Foundation, under Grant ECCS 2512911.

Corresponding author: Rui Zhang.

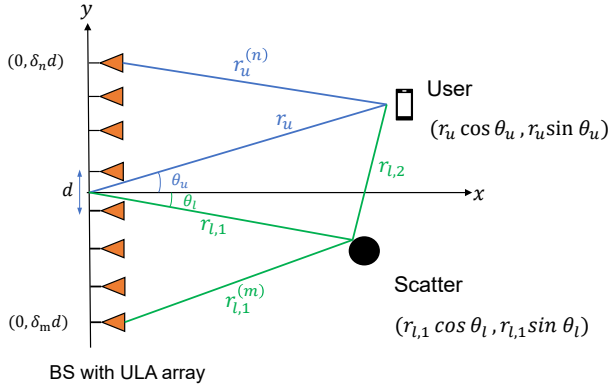


Fig. 1. Diagram of the near-field communication system featuring a ULA.

single-antenna user equipment (UE), as illustrated in Fig. 1. The boundary between the far-field and near-field regions is typically characterized by the Fresnel distance  $R_{\text{Fre}} = \frac{1}{2}\sqrt{\frac{D^3}{\lambda}}$  and the Rayleigh distance  $R_{\text{Ray}} = \frac{2D^2}{\lambda}$  [18]. Here,  $\lambda$  denotes the carrier wavelength and  $D = (N-1)d$  represents the physical aperture of the ULA, where  $d$  is the inter-element spacing. The system geometry is depicted in Fig. 1. The ULA is aligned along the  $y$ -axis and centered at the origin  $(0, 0)$ . The  $n$ -th antenna element is located at  $(0, \delta_n d)$ , where  $\delta_n = \frac{2n-N+1}{2}$  for  $n \in \mathcal{N} \triangleq \{0, 1, \dots, N-1\}$ . Assuming the standard spacing  $d = \frac{\lambda}{2}$ , the near-field steering vector for a target (UE or scatterer) at distance  $r$  and angular direction  $\theta$  is defined as:

$$\mathbf{b}(\theta, r) = \frac{1}{\sqrt{N}} \left[ e^{-j\frac{2\pi(r(0)-r)}{\lambda}}, \dots, e^{-j\frac{2\pi(r(N-1)-r)}{\lambda}} \right]^T, \quad (1)$$

where  $r$  is the distance from the UE or scatterer to the array center, and  $\theta \triangleq \sin(\varphi)$ , with  $\varphi$  being the angle of departure (AoD). The distance between the  $n$ -th element and the target is given by  $r^{(n)} = \sqrt{r^2 + \delta_n^2 d^2 - 2r\delta_n d\theta}$ .

We consider a multipath channel comprising  $L$  total paths. For a user located at  $(\theta_u, r_u)$ , the Line-of-Sight (LoS) component is modeled as

$$\mathbf{h}_{\text{LoS}} = \sqrt{N} g_u e^{-j\frac{2\pi r_u}{\lambda}} \mathbf{b}(\theta_u, r_u), \quad (2)$$

where  $g_u = \frac{\lambda}{4\pi r_u}$  denotes the path loss gain. The Non-Line-of-Sight (NLoS) component involves  $L-1$  scatterers and is expressed as

$$\mathbf{h}_{\text{NLoS}} = \sqrt{N} \sum_{l=1}^{L-1} g_l e^{-j\frac{2\pi(r_{l,1}+r_{l,2})}{\lambda}} \mathbf{b}(\theta_l, r_{l,1}), \quad (3)$$

where the  $l$ -th scatterer is positioned at  $(\theta_l, r_{l,1})$  and its distance to the user is  $r_{l,2} = \sqrt{r_{l,1}^2 + r_u^2 - 2r_{l,1}r_u \cos(\theta_u - \theta_l)}$  via the law of cosines. The complex gain  $g_l = \frac{\lambda p_l}{4\pi(r_{l,1}+r_{l,2})}$  accounts for path loss and the random reflection coefficient  $p_l \sim \mathcal{CN}(0, 1)$ . Consequently, the total multi-path channel model is given by

$$\mathbf{h} = \mathbf{h}_{\text{LoS}} + \mathbf{h}_{\text{NLoS}}. \quad (4)$$

Given the channel model in (4), the received signal  $y$  at a

user located at  $(\theta_u, r_u)$  is formulated as:

$$y(\mathbf{w}) = \mathbf{h}^H \mathbf{w} x + n, \quad (5)$$

where  $\mathbf{w} \in \mathbb{C}^{N \times 1}$  denotes the beamforming vector and  $n \sim \mathcal{CN}(0, \sigma^2)$  represents the complex additive white Gaussian noise (AWGN). Without loss of generality, the reference pilot signal is set to  $x = 1$ .

To exploit the spatial correlation of array responses in the angular domain, we introduce a unitary DFT matrix  $\mathbf{F} \in \mathbb{C}^{N \times N}$ . We define the DFT-domain channel coefficient vector  $\mathbf{g}$ , which is related to the spatial-domain channel vector  $\mathbf{h}$  by:

$$\mathbf{h} = \mathbf{F}^H \mathbf{g}. \quad (6)$$

The unitary DFT matrix is defined as  $\mathbf{F} = [\mathbf{a}(\varphi_0), \mathbf{a}(\varphi_1), \dots, \mathbf{a}(\varphi_{N-1})]$ , where the angles  $\varphi_n$  are uniformly sampled such that  $\varphi_n = \frac{2n-N+1}{N}$  for  $n \in \mathcal{N}$ . The  $n$ -th column of  $\mathbf{F}$  is given by:

$$\begin{aligned} \mathbf{a}(\varphi_n) &\triangleq \frac{1}{\sqrt{N}} \left[ e^{-j\pi(-\frac{N-1}{2})\varphi_n}, \dots, e^{-j\pi(\frac{N-1}{2})\varphi_n} \right]^T, \forall n \in \mathcal{N}. \end{aligned} \quad (7)$$

Substituting (6) into (5) yields a linear Gaussian observation model for the DFT-domain channel  $\mathbf{g}$ :

$$y_t = \mathbf{g}^H \mathbf{v}_t + n_t, \quad \mathbf{v}_t \triangleq \mathbf{F} \mathbf{w}_t. \quad (8)$$

### III. TS-BASED BEAM TRAINING SCHEME

We assume that the near-field channel vector  $\mathbf{h} \in \mathbb{C}^N$  remains quasi-static over a beam training interval consisting of  $T$  time slots. This training process is modeled as a linear Bandit problem, where the objective is to maximize the cumulative reward, and by extension, the spectral efficiency, through sequential decision-making. Specifically, in each slot  $t \in \{1, \dots, T\}$ , the BS selects a beamforming vector  $\mathbf{w}_t^*$  based on the history of previous observations.

To facilitate Thompson Sampling (TS), we treat the DFT-domain channel coefficient vector  $\mathbf{g}$  as a complex Gaussian random vector. We initialize the process with an angularly correlated prior distribution:

$$\tilde{\mathbf{g}}_0 \sim \mathcal{CN}(\mathbf{m}_0, \mathbf{D}_0). \quad (9)$$

Unlike far-field communications, where the energy of a single path can be tightly focused onto one DFT codeword, near-field communications often exhibit energy spread: a single near-field path component is typically distributed across multiple adjacent angular bins, as noted in [19]. This phenomenon implies that the elements of channel coefficient vector  $\mathbf{g}$  within the DFT-domain are not independent but exhibit correlation with their neighbors. Fig. 2a illustrates this effect, showing the normalized power distribution across the angular domain in a multipath environment ( $L=4$ ). The UE's angle is  $\varphi_u = 0$  and AoD of other three scatterers are  $\varphi_1 = -\frac{\pi}{4}$ ,  $\varphi_2 = \frac{\pi}{6}$ ,  $\varphi_3 = \frac{\pi}{3}$ .

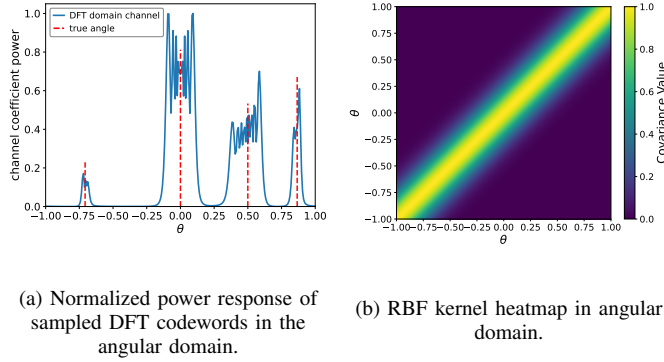


Fig. 2. Influence of power leakage on the angular domain and the corresponding RBF kernel.

To mathematically capture this angular-domain dependence of the channel in DFT domain, we adopt a Gaussian (RBF) kernel to define the prior covariance matrix  $\mathbf{D}_0$ :

$$[\mathbf{D}_0]_{i,j} = \exp\left(-\frac{1}{2} \left(\frac{\varphi_i - \varphi_j}{\ell}\right)^2\right), \quad (10)$$

where the hyperparameter  $\ell$  controls the correlation length along the angular grid. As depicted in Fig. 2b, this prior encodes the physical intuition that neighboring angular components are statistically dependent, allowing the BS to learn about adjacent beams even when they are not explicitly probed.

Let  $\mathcal{H}_{t-1} \triangleq \{(\mathbf{v}_\tau, y_\tau)\}_{\tau=1}^{t-1}$  represent the observation history up to slot  $t$ . The posterior distribution of  $\mathbf{g}$ , given the history, is modeled as a complex Gaussian distribution:

$$\tilde{\mathbf{g}}_t \mid \mathcal{H}_{t-1} \sim \mathcal{CN}(\mathbf{m}_{t-1}, \mathbf{D}_{t-1}). \quad (11)$$

At time slot  $t$ , we sample from the posterior distribution given by Eq. (11) and map the sampled DFT-domain vector to beamspace via Eq. (6). This beamspace sample  $\tilde{\mathbf{h}}_t$  is then used (directly or through a codebook) to select the transmit beamformer  $\mathbf{w}_t^*$  for slot  $t$ . After transmitting  $\mathbf{w}_t^*$  and observing the resulting signal  $y_t$ , the belief (mean and covariance of the posterior distribution) is updated iteratively. This framework transforms the beam training task into a sequential search: in each slot, we sample from the current belief to choose a beam and subsequently refine that belief based on the new observation.

We leverage TS to adaptively trade off exploration and exploitation by drawing samples from the posterior distribution in Eq. (11). In the Gaussian distribution, the covariance  $\mathbf{D}_{t-1}$  quantifies the uncertainty of  $\tilde{\mathbf{g}}_t$  at time  $t$ . Its diagonal elements, in particular, are the variances of the corresponding elements in  $\tilde{\mathbf{g}}_t$ . Unlike other algorithms, such as UCB, TS inherently balances exploration and exploitation via randomness drawn from the posterior. When posterior variances are large, TS more frequently proposes diverse beam candidates (promoting exploration). As the posterior concentrates, TS draws concentrate near the posterior mean, and the algorithm naturally favors exploitation.

Through iterative sampling and Bayesian updates, the estimated channel vector  $\tilde{\mathbf{h}}_t$  adaptively converges toward the optimal channel coefficient vector  $\mathbf{h}^*$  as  $t$  grows. Convergence

is declared if the received signal magnitude remains within a tolerance  $\varepsilon$  for  $t'$  consecutive transmissions:

$$|y_t| - |y_{t-1}| \leq \varepsilon \quad \text{for } t' \text{ consecutive slots.} \quad (12)$$

We consider three TS-based beam-training schemes for selecting the transmit beam during training process.

- **Scheme I (Codebook-constrained TS).** The action set of beam sweeping in this case is restricted to the near-field codebook  $\mathcal{W}$  defined in [8]. This near-field codebook is constructed in the polar domain using uniform angular sampling and non-uniform distance sampling. For each sweeping time slot, TS selects the codeword that maximizes its inner product with the sampled channel from the posterior distribution:

$$\mathbf{w}_t^* = \arg \max_{\mathbf{w} \in \mathcal{W}} |\tilde{\mathbf{h}}_t^H \mathbf{w}|, \quad (13)$$

After convergence at time slot  $T'$ , the data beam is constructed from the latest posterior mean as  $\mathbf{m}_{T'}$

$$\mathbf{w}_{\text{data}} = \frac{\mathbf{F}^H \mathbf{m}_{T'}}{\|\mathbf{F}^H \mathbf{m}_{T'}\|_2}. \quad (14)$$

The near-field codebook provides an intrinsic regularization effect. By constraining the search space, Scheme I prevents the beam from deviating due to initial channel uncertainty, thereby accelerating convergence, particularly in low SNR regimes where prior information is limited.

- **Scheme II (Continuous Space TS).** Different from scheme I, the action set of beam sweeping is the full unit sphere  $\mathcal{W}_{\text{cont}} = \{\mathbf{w} \in \mathbb{C}^N : \|\mathbf{w}\|_2 = 1\}$ . TS directly uses the normalized sampled channel for the beam training:

$$\mathbf{w}_t^* = \frac{\tilde{\mathbf{h}}_t}{\|\tilde{\mathbf{h}}_t\|_2}. \quad (15)$$

After convergence, the data beam is constructed in the same way as Eq. (14). While Scheme II is theoretically capable of achieving full CSI by exploring the continuous space, it may suffer from slower convergence. In the absence of codebook-based guidance, significant resources may be spent on sub-optimal exploration during the initial stages when the channel estimate is highly uncertain.

- **Scheme III (Hybrid refinement TS).** To consolidate the advantages of both approaches, we propose a Hybrid TS scheme that operates in two consecutive stages. In Stage 1, it follows Scheme I and performs TS-based beam training over the codebook  $\mathcal{W}$  according to Eq. (13). This exploits the regularization of the codebook to quickly stabilize the search. Once Stage 1 converges, the action set switches to the continuous space  $\mathcal{W}_{\text{cont}}$ . The beamformer is then refined via Eq. (15) to capture the full CSI. Once the channel estimate converges in the second stage at time slot  $T'$ , the data beam is formed using Eq. (14). This hybrid approach effectively uses the codebook to "warm-start" the estimation process, ensuring rapid initial convergence before transitioning to a continuous search for maximum precision.

**Algorithm 1** Proposed TS-based Beam Training Framework

**Input:** NF Codebook  $\mathcal{W}$ , DFT matrix  $\mathbf{F}$ , Prior information  $\mathbf{m}_0, \mathbf{D}_0$ , Max slots  $T$ , Tolerance  $\varepsilon$ , stop criterion  $t'$ .

**Output:** Data beamformer  $\mathbf{w}_{\text{data}}$ 

- 1:  $t \leftarrow 1$
- 2: **while**  $t \leq T$  **do**
- 3: Sample  $\tilde{\mathbf{g}}_t$  via Eq.(11) and map to spatial domain channel vector  $\tilde{\mathbf{h}}_t$  by Eq. (6).
- 4: Construct beamformer  $\mathbf{w}_t^*$  via Eq.(13) or Eq. (15).
- 5: Transmit  $\mathbf{w}_t^*$  and get observation  $y_t$ .
- 6: Update posterior mean and covariance  $(\mathbf{m}_t, \mathbf{D}_t)$  via Eq. (16) - Eq. (19).
- 7: **if** converge at (12) **then**
- 8:     **break**
- 9: **end if**
- 10:  $t \leftarrow t + 1$
- 11: **end while**
- 12: **return**  $\mathbf{w}_{\text{data}}$  via Eq.(14).

All three schemes share the same Bayesian update rules. After transmitting  $\mathbf{w}_t^*$  and receiving the observation  $y_t$ , we set  $\mathbf{v}_t = \mathbf{F}\mathbf{w}_t^*$  and update the posterior mean and covariance  $(\mathbf{m}_{t-1}, \mathbf{D}_{t-1}) \mapsto (\mathbf{m}_t, \mathbf{D}_t)$  as follows:

$$\alpha_t \triangleq \mathbf{v}_t^H \mathbf{D}_{t-1} \mathbf{v}_t + \sigma^2, \quad (16)$$

$$\mathbf{k}_t \triangleq \frac{\mathbf{D}_{t-1} \mathbf{v}_t}{\alpha_t}, \quad (17)$$

$$\mathbf{m}_t = \mathbf{m}_{t-1} + \mathbf{k}_t (y_t - \mathbf{v}_t^H \mathbf{m}_{t-1}), \quad (18)$$

$$\mathbf{D}_t = \mathbf{D}_{t-1} - \mathbf{k}_t \mathbf{v}_t^H \mathbf{D}_{t-1}. \quad (19)$$

In summary, the proposed TS-based framework uses various schemes and a closed-form Bayesian recursion Eq. (16) – Eq. (19) to update the distribution of  $\tilde{\mathbf{g}}_t$  after each observation. Upon completion of training, the final beamformer  $\mathbf{w}_{\text{data}}$  is selected for data transmission.

## IV. SIMULATION RESULTS AND ANALYSIS

To evaluate the proposed schemes, we consider a BS equipped with  $N = 256$  antenna elements operating at a carrier frequency of 30 GHz. The channel model comprises  $L = 4$  paths, consisting of one LoS and three NLoS components. The user and scatterers are randomly distributed within a distance range of  $[7, 100]$  m and an angular range of  $[-\pi/3, \pi/3]$ . We employ the near-field polar codebook  $\mathcal{W}$  from [8] with an expansion factor  $\beta = 1.1$ , resulting in a total of 1280 codewords. For the TS-based beam training, the convergence threshold is set to  $\epsilon = 1 \times 10^{-7}$  over  $t' = 10$  consecutive transmissions, and the maximum pilot limit is  $T = 1280$  (matching the codebook size). Besides, we set  $\ell = 1/128$  to control the angular correlation length of the RBF kernel for prior covariance matrix. All results are averaged over  $N_{\text{iter}} = 500$  independent Monte-Carlo trials to ensure statistical robustness. The performance is quantified by the achievable rate, defined as:  $R = \log_2 \left( 1 + \frac{|\mathbf{w}_{\text{data}}^H \mathbf{h}|^2}{\sigma^2} \right)$ .

In this section, we evaluate the performance of the three proposed TS-based schemes alongside the multi-beam linear combination approach introduced in [17]. The latter performs an exhaustive beam sweep using a far-field DFT codebook and

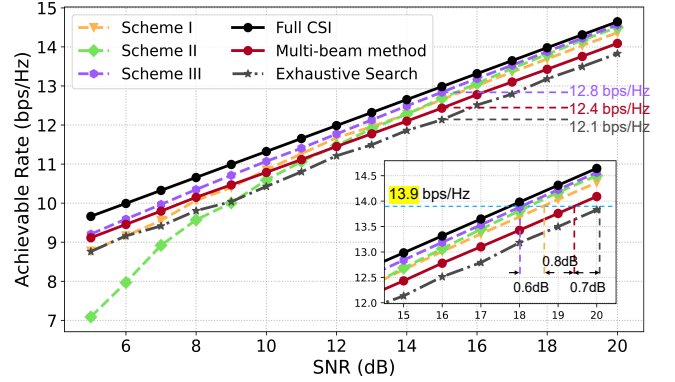


Fig. 3. Achievable rate performance vs. SNR of various schemes under finite maximum pilot overhead constraints.

subsequently constructs a new beamformer through a linear combination of the sampled beams that captures full channel information. For benchmarking, we also include two baselines: (i) the full CSI case, which serves as the theoretical upper bound, and (ii) a conventional exhaustive search over the near-field (NF) codebook  $\mathcal{W}$  that captures only the strongest path in the channel.

Fig. 3 illustrates the achievable rate versus SNR for the evaluated schemes, while Fig. 4 presents the corresponding training pilot overhead for SNR levels ranging from 5 to 20 dB. Both the proposed TS-based frameworks and the multi-beam method significantly outperform conventional exhaustive search due to their ability to capture multiple paths. Among the proposed approaches, the hybrid refinement TS (Scheme III) exhibits the most robust performance, maintaining the narrowest gap to the full-CSI upper bound across the entire SNR regime. Specifically, at an SNR of 15 dB, Scheme III achieves a rate of 12.8 bps/Hz, surpassing the multi-beam method (12.4 bps/Hz) and exhaustive search (12.1 bps/Hz). This spectral efficiency gain is achieved with an average pilot overhead of only 101.4, which is substantially lower than the 256 and 1280 pilots required by the multi-beam and exhaustive baselines, respectively. Furthermore, to attain a target achievable rate of 13.9 bps/Hz, Scheme III offers SNR gains of approximately 0.6 dB, 1.4 dB, and over 2 dB relative to Scheme I, the multi-beam baseline, and exhaustive NF codebook search, respectively.

Conversely, the continuous-space TS (Scheme II) suffers from severe performance degradation in the low-SNR regime. Its unconstrained exploration is highly susceptible to noise, often failing to reach convergence within the maximum iteration budget  $T$ , as illustrated in Fig. 4. However, as the SNR increases, Scheme II achieves convergence within the budget and eliminates the grid quantization errors inherent in discrete codebooks, eventually surpassing the codebook-constrained Scheme I. Ultimately, by leveraging codebook-based priors for rapid stabilization and continuous-space search for high-precision refinement, Scheme III consistently achieves superior performance across all benchmarks. It reduces pilot overhead by approximately 90% compared to a full NF codebook sweep. Notably, while the multi-beam benchmark necessitates a constant overhead of 256 pilots for its initial DFT-domain

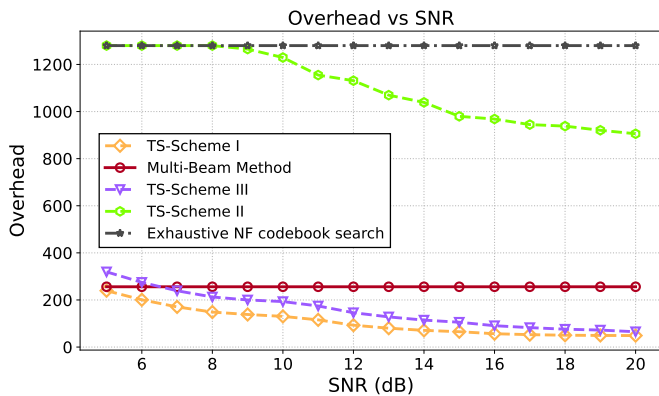


Fig. 4. Beam Training Pilot Overhead versus SNR of various schemes.

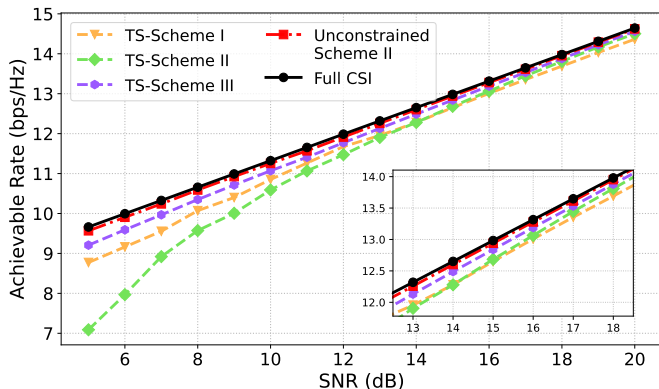


Fig. 5. Achievable rate versus SNR: Comparison between the unconstrained Scheme II and various schemes under finite pilot overhead constraints.

exhaustive search, the proposed TS framework dynamically reduces its sweeping duration, highlighting its superior pilot efficiency for latency-sensitive near-field communications.

To further characterize the fundamental potential of continuous-space exploration, Fig. 5 introduces an unconstrained benchmark, denoted as Unconstrained Scheme II. In this scenario, the maximum pilot budget  $T$  is removed, allowing the TS process to proceed until the convergence threshold  $\epsilon$  is strictly satisfied. By eliminating the pilot overhead constraint, the algorithm effectively mitigates its inherent noise sensitivity in the low-SNR regime through prolonged posterior refinement. As illustrated, the achievable rate of the unconstrained scheme asymptotically approaches the Full CSI upper bound across the entire SNR range. This convergence behavior confirms that the performance degradation observed in Fig. 3 is primarily a consequence of the limited pilot budget rather than a lack of estimation precision.

## V. CONCLUSION

This letter presented a linear bandit framework for efficient near-field beam training in XL-MIMO systems under multipath propagation. By leveraging Thompson Sampling in the DFT domain, we incorporated a Gaussian kernel-based prior to capture angular correlations and near-field energy leakage. Built upon Bayesian recursion, three strategies were developed: codebook-constrained search for rapid convergence, continuous-space search for high-precision alignment, and a hybrid scheme that balances both. Simulation results demon-

strate that the proposed framework reduces pilot overhead by approximately one order of magnitude relative to exhaustive sweeping baseline, while remaining robust in multipath environments. Notably, under the maximum pilot constraint, the hybrid scheme attains the highest achievable rate with a small overhead, offering up to a 0.47 bps/Hz gain over the multi-beam method. Moreover, the continuous-space strategy was shown to be asymptotically optimal, approaching the full-CSI bound as the pilot budget becoming unconstrained.

## REFERENCES

- [1] S. Kang et al., "Cellular wireless networks in the upper mid-band," *IEEE Open Journal of the Communications Society*, vol. 5, pp. 2058–2075, 2024.
- [2] J. M. Jornet, N. Yang, R. Nichols, S. Nie, C. Huang, and R. K. Mallik, "Terahertz communications and sensing for 6g and beyond: How far are we?" *IEEE Wireless Communications*, vol. 31, no. 1, pp. 8–9, 2024.
- [3] C.-X. Wang et al., "On the road to 6g: Visions, requirements, key technologies, and testbeds," *IEEE Communications Surveys & Tutorials*, vol. 25, no. 2, pp. 905–974, 2023.
- [4] A. Singh, P. Sen, J. Osmond, L. Chapagain, and S. Nie, "A novel feature of 6g: Asymmetric uplink/downlink channels in the terahertz near field-modeling and characterization," in *ICC 2025-IEEE International Conference on Communications*, IEEE, 2025, pp. 1754–1759.
- [5] A. Rasteh, R. P. Hari, H. Guo, M. Mezzavilla, and S. Rangan, "Near-field measurement system for the upper mid-band," in *2024 58th Asilomar Conference on Signals, Systems, and Computers*, 2024, pp. 1684–1689.
- [6] H. Zhang, N. Shlezinger, F. Guidi, D. Dardari, et al., "Beam focusing for near-field multi-user MIMO communications," *IEEE Transactions on Wireless Communications*, vol. 21, no. 9, pp. 7476–7490, 2022.
- [7] X. Wei and L. Dai, "Channel estimation for extremely large-scale massive MIMO: Far-field, near-field, or hybrid-field?" *IEEE Communications Letters*, vol. 26, no. 1, pp. 177–181, 2022.
- [8] M. Cui and L. Dai, "Channel estimation for extremely large-scale MIMO: Far-field or near-field?" *IEEE Transactions on Communications*, vol. 70, no. 4, pp. 2663–2677, 2022.
- [9] Y. Liu, Z. Wang, J. Xu, C. Ouyang, X. Mu, and R. Schober, "Near-field communications: A tutorial review," *IEEE Open Journal of the Communications Society*, vol. 4, pp. 1999–2049, 2023.
- [10] M. Cui, Z. Wu, Y. Lu, X. Wei, and L. Dai, "Near-field MIMO communications for 6G: Fundamentals, challenges, potentials, and future directions," *IEEE Communications Magazine*, vol. 61, no. 1, pp. 40–46, 2023.
- [11] J. Chen, F. Gao, M. Jian, and W. Yuan, "Hierarchical codebook design for near-field mmwave mimo communications systems," *IEEE Wireless Communications Letters*, vol. 12, no. 11, pp. 1926–1930, 2023.
- [12] C. Wu, C. You, Y. Liu, L. Chen, and S. Shi, "Two-stage hierarchical beam training for near-field communications," *IEEE Transactions on Vehicular Technology*, vol. 73, no. 2, pp. 2032–2044, 2023.
- [13] X. Wu, C. You, J. Li, and Y. Zhang, "Near-field beam training: Joint angle and range estimation with dft codebook," *IEEE Trans. Wireless Commun.*, vol. 23, no. 9, pp. 11 890–11 903, Sep. 2024.
- [14] Z. Wang, R. Kiran, S. Tsai, and R. Zhang, "Low-complexity near-field beam training with dft codebook based on beam pattern analysis," *accepted by IEEE Globecom 2025*, Mar. 2025. arXiv: 2503.21954 [eess.SP].
- [15] Z. Xu, Z. Zhang, and L. Dai, "Near-optimal near-field beam training: From searching to inference," *IEEE Transactions on Wireless Communications*, vol. 24, no. 11, pp. 9173–9185, 2025.
- [16] W. Wu, N. Cheng, N. Zhang, P. Yang, W. Zhuang, and X. Shen, "Fast mmwave beam alignment via correlated bandit learning," *IEEE Transactions on Wireless Communications*, vol. 18, no. 12, pp. 5894–5908, 2019.
- [17] Z. Wang et al., "Sparsity-aware near-field beam training via multi-beam combination," *Accepted by IEEE Globecom 2025, arXiv preprint arXiv:2505.08267*, 2025. arXiv: 2505.08267 [cs.IT].
- [18] K. T. Selvan and R. Janaswamy, "Fraunhofer and fresnel distances: Unified derivation for aperture antennas," *IEEE antennas and propagation magazine*, vol. 59, no. 4, pp. 12–15, 2017.
- [19] M. Cui, Z. Wu, Y. Lu, X. Wei, and L. Dai, "Near-field wideband beamforming for extremely large antenna arrays," *IEEE Transactions on Wireless Communications*, vol. 21, no. 9, pp. 7125–7138, 2022.